First-principles description of the exciton-phonon interaction: A cumulant approach

Pierluigi Cudazzo
Physics and Materials Science Research Unit, University of Luxembourg, 162a avenue de la Faïencerie, L-1511 Luxembourg, Luxembourg and European Theoretical Spectroscopy Facility (ETSF)

(Received 26 March 2020; revised 5 July 2020; accepted 6 July 2020; published 23 July 2020)

Electron-phonon coupling leads to intriguing effects in the spectra of materials. Current approximations to calculate spectra most often describe this coupling insufficiently. Starting from basic equations of many-body perturbation theory, we derived a cumulant formulation for neutral excitation spectra that contains excitonic effects and the coupling between excitons and phonons. The cumulant approach allows us to include dynamical effects arising from the electron-phonon coupling in a simple and intuitive way. It can be implemented as a postprocessing of state-of-the-art *GW*-plus-Bethe-Salpeter calculation of excitonic states and a density functional perturbation theory calculation of phonons and electron-phonon coupling. We demonstrate that, in order to obtain a consistent treatment of exciton-phonon coupling, diagrams have to be taken into account that can be neglected when the effect of lattice vibrations is treated in a static or quasistatic approximation. From the application of this approach to a model system, we analyzed the main features of the exciton-phonon interaction and provided a general picture of their link with the properties of materials such as exciton mass and exciton Bohr radius.

DOI: 10.1103/PhysRevB.102.045136

I. INTRODUCTION

The electron-phonon (el-ph) interaction is central to a wide range of phenomena in materials physics [1]. For example, it underpins the temperature dependence of the electrical resistivity in metals and the carrier mobility in semiconductors, gives rise to conventional superconductivity, and sets the relaxation processes of excited states. Moreover, the el-ph interaction often affects the excitation spectra measured, for example, in photoemission and absorption spectroscopies. In those spectra, it induces shifts and broadening of peaks as well as additional structures called satellites. Those effects dominate the photoluminescence and the low-energy optical spectra of indirect-gap semiconductors [2–5], and they play a key role in the understanding of the electronic and optical properties of molecular crystals [6], quantum dots [7], and polaronic systems such as transition metal oxides [8,9] and ionic crystals [10].

The effect of el-ph interaction has been investigated extensively in the past using model Hamiltonians [11–14] often combined with the polaronic picture [15], and it still attracts considerable attention. Models are often not predictive and difficult to combine with *ab initio* calculations. On the contrary, many-body perturbation theory (MBPT) [16–19] represents a reliable and accurate approach for the description of excited states and is thus the ideal framework to investigate the effect of el-ph interaction on the excitation spectra [1].

In MBPT the key quantities are Green's functions. The one-particle Green's function G gives direct access to one-particle excitations measured by photoemission, while the two-particle correlation function L yields neutral excitations probed in optical absorption, electron energy loss, and inelastic x-ray scattering experiments. In this framework, all many-body effects induced by the Coulomb and el-ph interactions are included through the electron self-energy Σ [1,18,19]. It defines both the kernel of the Dyson equation for G, and an effective electron-hole (e-h) interaction that is the kernel of the Bethe-Salpeter equation (BSE) for L [18,19].

In state-of-the-art calculations of the one-particle Green's function [1], the el-ph interaction is treated within the Heine-Allen-Cardona (HAC) scheme [20,21], which consists of a second-order expansion of the electron self-energy in terms of the el-ph coupling constant. This approach has been successfully applied to the study of the temperature dependence of quasiparticle (QP) gap in insulators [22–25] and semiconductors [26,27], and it has been extended to the BSE for optical spectra [28]. However, although the HAC scheme provides an accurate description of QP excitations and their lifetime, it often fails to describe satellites in photoemission spectra [8,9,29]. Satellites are genuine dynamical effects that require both the full frequency dependence of the self-energy and the inclusion of higher-order corrections in the perturbative expansion of the Green's function [1,30]. This would make the solution of the Dyson equation inaccessible in real materials.

In the spectra of neutral excitations, satellites are completely missed by present-day approaches that treat the el-ph interaction within a static or quasistatic approximation [28] (i.e., neglecting the full frequency dependence of the electron self-energy). The fully dynamical BSE is extremely complicated to solve [31,32], and its solution might not be worth the effort. Indeed, the BSE with a first-order kernel is similar to the Dyson equation for G in the HAC scheme that often fails for satellites. Rather than a scheme based on a Dyson equation, a cumulant approach [33–35] for the two-particle

correlation function, reflecting a picture of coupled bosons, appears more promising. It is the exact solution for a two-level limiting case [36], and it is additionally motivated by the success of an increasing number of *ab initio* calculations for G using a cumulant of second order in the el-ph coupling [37–40]. This promising approach was recently formulated for the two-particle correlation function in order to include correlation effects arising from the dynamically screened Coulomb interaction and neglected in standard BSE calculations [41]. The formulation of Ref. [41] is general and in principle can be extended to describe the coupling between excitons and any kind of bosonic excitation such as free electron-hole pairs, other excitons, plasmons, photons, as well as phonons.

In this paper, motivated by these recent developments, we derive the cumulant expression for the two-particle correlation function in the presence of el-ph interaction. In particular, following Ref. [41], the derivation is done in two main steps. First of all, starting from the fully dynamical BSE we obtained a Dyson-like equation for the two-time charge-charge response function that represents the exciton propagator and provides the spectrum of neutral excitations. This requires the introduction of an exciton self-energy related to the el-ph interaction. At this point, the cumulant expression for the exciton propagator comes out naturally. Indeed, in analogy with the one-particle Green's function [42], the cumulant coefficient is obtained imposing that the first-order expansion of a cumulant ansatz for the exciton propagator matches the first-order expansion of the Dyson equation. Our method is applied to a simple model system that is used as an illustrative example to discuss the basic physical aspects of the cumulant in a general way.

II. PERTURBATIVE EXPANSION OF THE TWO-PARTICLE CORRELATION FUNCTION

In the framework of MBPT, the two-particle correlation function L is formally obtained from the solution of the BSE [18,19]:

$$L(1423) = L_0(1423) + L_0(14'21')\frac{\delta\Sigma(1'2')}{\delta G(3'4')}L(3'42'3). \quad (1)$$

Here 1 stands for space, spin, and time ($\mathbf{r}_1\sigma_1 t_1$), and repeated indices are integrated over. The quantity $L_0(14'21') \equiv G(11')G(4'2)$ is the uncorrelated two-particle Green's function, while the kernel is the functional derivative of the self-energy Σ with respect to the one-particle Green's function G. Σ can be formally split in a purely electronic part and a contribution related to the coupling with phonons. The electronic part is the sum of the Hartree contribution Σ_H and the Coulomb exchange-correlation term $\Sigma^C_{\rm xc}$ that in state-of-the-art calculations is evaluated in the static COulomb Hole plus Screened EXchange (COHSEX) approximation (or eventually quasiparticle GW approximation) [19,43]. According to the HAC scheme [20,21], the el-ph contribution can be split in a static Debye-Waller term $\Sigma_{\rm DW}$ and an exchange-correlation term $\Sigma^{\rm ph}_{\rm xc}$ related to the dynamical fluctuation of the lattice. The latter can be perturbatively expanded in terms of the nuclear contribution ($W^{\rm ph}$) to the screened Coulomb interaction [1]. At the first order in $W^{\rm ph}$ (i.e., second order in the el-ph coupling), $\Sigma^{\rm ph}_{\rm xc}$ reduces to the Fan-Migdal (FM) term that is used in state-of-the-art calculations [1,28]. Moreover, both $\Sigma_{\rm DW}$ and $W^{\rm ph}$ can be written in terms of the el-ph matrix elements and the phonon propagator that we assume to be known.

In the standard approach, i.e., in the absence of el-ph interaction and with an instantaneous kernel, the BSE can be rewritten directly in terms of two-time $L_0(\mathbf{r}_1 t_1 \mathbf{r}_4 t_3 \mathbf{r}_2 t_1 \mathbf{r}_3 t_3)$. Under these conditions, the BSE becomes a Dyson-like equation that can be directly solved in two times or one frequency [19]. In the present case, instead, because of the explicit time dependence of $W^{\rm ph}$, Eq. (1) cannot be rewritten in terms of a two-time propagator only, and it is hardly solvable even considering the simplest first-order $W^{\rm ph}$ expansion for Σ.

In the following, we will rearrange Eq. (1) in such a way as to obtain an approximate Dyson-like equation for L that allows including simultaneously dynamical effects related to $W^{\rm ph}$ and excitonic effects related to the Coulomb interaction. This is a necessary step to include a QP correction to the exciton energy and find a cumulant representation for L. First of all, we rewrite Eq. (1) as

$$\begin{aligned} L(1423) = \bar{L}(1423) + \bar{L}(12'21')\big[&\Xi_1(1'4'2'3') \\ &+ L_0^{0,-1}(1'4'2'3') \\ &- (L_0^0 + L_0^1)^{-1}(1'4'2'3')\big]L(3'44'3), \end{aligned} \quad (2)$$

where we have split both $L_0(1423)$ and the kernel $\Xi(1423) = \frac{\delta\Sigma(12)}{\delta G(34)}$ into two parts: $L_0 = L_0^0 + L_0^1$ and $\Xi = \Xi_0 + \Xi_1$. Here $(L_0^0 + L_0^1)^{-1}(1423)$ denotes the inverse of $L_0^0(1423) + L_0^1(1423)$, and $\bar{L}$ is the solution of

$$\bar{L}(1423) = L_0^0(1423) + L_0^0(12'21')\Xi_0(1'4'2'3')\bar{L}(3'44'3). \quad (3)$$

Up to here, the splitting has been arbitrary. We choose $\Xi_0(1423) \equiv -iv(13)\delta(12)\delta(34) + iW_0^C(12)\delta(13)\delta(24)$, where v is the bare Coulomb potential and $W_0^C(12) = W^C(12)\delta(t_2 - t_1)$ is the statically screened Coulomb potential. Moreover, we set $L_0^0(1423) \equiv \bar{G}(13)\bar{G}(42)$, where $\bar{G}$ is the one-body Green's function evaluated in the COHSEX approximation and eventually dressed by $\Sigma_{\rm DW}$.

This definition for $\bar{G}$ is consistent with our choice for Ξ_0. With this choice, Eq. (3) is the static BSE (SBSE) with el-ph interaction treated in the static approximation (i.e., including only the Debye-Waller term). By construction, the kernel of Eq. (2) describes dynamical effects induced by el-ph coupling beyond the SBSE.

We now expand this kernel to first order in $W^{\rm ph}$. The first-order correction to the self-energy is just the FM term $\Sigma_{\rm FM}(12) = iW^{\rm ph}(12)\bar{G}(12)$, which leads to first-order correction to the Green's function $G^1(12) = \bar{G}(11')\Sigma_{\rm FM}(1'2')\bar{G}(2'2)$. This leads to

$$\begin{aligned} L_0^1(1423) = &\bar{G}(13)\bar{G}(44')\Sigma_{\rm FM}(4'2')\bar{G}(2'2) \\ &+ \bar{G}(11')\Sigma_{\rm FM}(1'3')\bar{G}(3'3)\bar{G}(42), \end{aligned} \quad (4)$$

and, through the expansion of the inverse, to

$$\begin{aligned} L(1423) = \bar{L}(1423) + \bar{L}(12'21')\big[&\Xi_1(1'4'2'3') \\ &+ L_0^{0,-1}(1'52'6)L_0^1(6857)L_0^{0,-1}(74'83')\big]\bar{L}(3'44'3). \end{aligned} \quad (5)$$

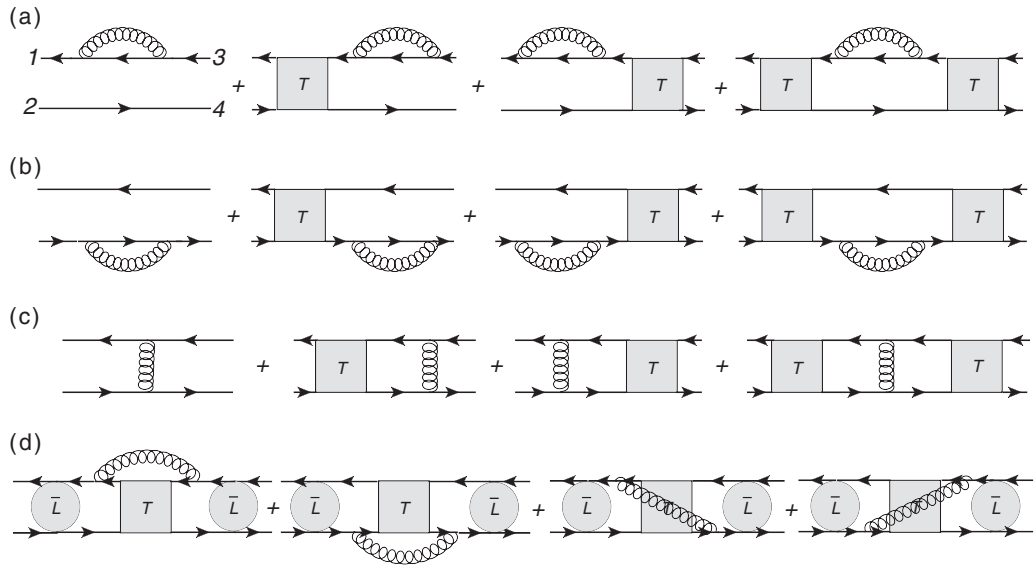

FIG. 1. Feynman diagrams associated with the first-order expansion L in terms of $W^{\rm ph}$. They involve diagrams associated with the term $L_0^{0,-1}L_0^1L_0^{0,-1}$ [(a) and (b)] and diagrams arising from the kernel Ξ_1 defined in Eq. (8) [(c) and (d)]. Arrows are the one-particle Green's function $\bar{G}$, the gray circles indicate $\bar{L}$, the gray boxes denote the T matrix, and wiggly lines correspond to $W^{\rm ph}$.

To be consistent, we also use the first order in $W^{\rm ph}$ expression for Ξ_1, which can be obtained from $\frac{\delta\Sigma_{\rm FM}}{\delta\bar{G}} = iW^{\rm ph}$. This gives the first-order $W^{\rm ph}$ diagrams for L shown in Figs. 1(a)–1(c), where we used the following representation for $\bar{L}$:

$$\bar{L}(1423) = L_0^0(1423) + L_0^0(1\bar{2}2\bar{1})T(\bar{1}4\bar{2}\bar{3})L_0^0(\bar{3}4\bar{4}3) \quad (6)$$

in terms of the T-matrix defined as [18]

$$T(1423) = \Xi_0(1423) + \Xi_0(1\bar{2}2\bar{1})L_0^0(\bar{1}4\bar{2}\bar{3})T(\bar{3}4\bar{4}3). \quad (7)$$

In particular, the class of diagrams in Figs. 1(a) and 1(b) and Fig. 1(c) arises from $L_0^{0,-1}L_0^1L_0^{0,-1}$ and Ξ_1, respectively. It describes an exciton that, through the emission (absorption) of a phonon scatters in an intermediate state consisting of a noninteracting electron-hole pair. This approximation is formally equivalent to the Shindo treatment of the el-ph interaction in the case of shallow excitons [44]. However, since $W^{\rm ph}$ is not instantaneous, as pointed out in Ref. [41] in the case of dynamically screened Coulomb interaction, there is no reason to neglect the class of first-order diagrams shown in Fig. 1(d). They take into account excitonic effects in the intermediate states, and they can be included by considering the following first-order expression for Ξ_1:

$$\begin{aligned}\Xi_1(1423) = {} & iW^{\rm ph}(23)T(14\bar{2}\bar{3})\bar{G}(\bar{3}3)\bar{G}(\bar{2}2)\\ & + iW^{\rm ph}(14)T(\bar{1}4\bar{2}3)\bar{G}(1\bar{1})\bar{G}(4\bar{4})\\ & + iW^{\rm ph}(42)T(1\bar{4}\bar{2}3)\bar{G}(\bar{2}2)\bar{G}(4\bar{4})\\ & + iW^{\rm ph}(13)T(\bar{1}4\bar{2}\bar{3})\bar{G}(\bar{3}3)\bar{G}(1\bar{1})\\ & + iW^{\rm ph}(12)\delta(13)\delta(24). \end{aligned} \quad (8)$$

Inserting Eq. (8) and Eq. (4) into Eq. (5), we obtain

$$L(1423) = \bar{L}(1423) + \bar{L}(12'21')\mathcal{K}(1'4'2'3')\bar{L}(3'44'3), \quad (9)$$

with the new kernel

$$\begin{aligned}\mathcal{K}(1423) = {} & iW^{\rm ph}(14)\bar{L}(14\bar{2}\bar{3})\bar{G}^{-1}(\bar{3}3)\bar{G}^{-1}(\bar{2}2)\\ & + iW^{\rm ph}(32)\bar{L}(\bar{1}4\bar{2}3)\bar{G}^{-1}(1\bar{1})\bar{G}^{-1}(4\bar{4})\\ & + iW^{\rm ph}(13)\bar{L}(1\bar{4}\bar{2}3)\bar{G}^{-1}(\bar{2}2)\bar{G}^{-1}(4\bar{4})\\ & + iW^{\rm ph}(42)\bar{L}(\bar{1}4\bar{2}\bar{3})\bar{G}^{-1}(\bar{3}3)\bar{G}^{-1}(1\bar{1}). \end{aligned} \quad (10)$$

The diagrammatic representation of L in Fig. 1 illustrates that we include the complete series of ladder diagrams in the effective four-point Coulomb interaction Ξ_0 responsible for excitonic effects, whereas the dynamical el-ph interaction is included through an effective kernel evaluated at the first order in $W^{\rm ph}$. Under the assumption that elementary scattering processes between occupied and empty states are negligible, which corresponds to the Tamm-Dancoff approximation (TDA) [16,45,46] for both $\bar{L}$ and the scattering processes induced by $W^{\rm ph}$, Eq. (5) is the exact expression for the first-order $W^{\rm ph}$ expansion of L.

III. EXCITON SELF-ENERGY AND CUMULANT COEFFICIENT

Our next goal is to express Eq. (9) in terms of the two-time e-h correlation function $\bar{\mathcal{G}}(\mathbf{r}_1t_1\mathbf{r}_4t_3\mathbf{r}_2t_1\mathbf{r}_3t_3) = -i\bar{L}(\mathbf{r}_1t_1\mathbf{r}_4t_3\mathbf{r}_2t_1\mathbf{r}_3t_3)$ and $W^{\rm ph}$. $\bar{\mathcal{G}}$ represents the noninteracting exciton Green's function. When evaluated at $\mathbf{r}_2 = \mathbf{r}_1$ and $\mathbf{r}_4 = \mathbf{r}_3$ it corresponds to the charge-charge response function from the SBSE. We want now to obtain an expression for the full charge-charge response function $\mathcal{G}$ in the presence of el-ph interaction. In analogy to the one-particle G for one-particle excitations, $\mathcal{G}$ represents an interacting Green's function for the exciton, i.e., an exciton propagator. To this end, we first note that the diagrammatic series obtained from Eq. (9) can be traced back to the two prototypical Feynman diagrams drawn in Figs. 2(a) and 2(b) evaluated at all orders in Ξ_0. At first glance, it is impossible to detect the two-times $\bar{\mathcal{G}}$ in the black

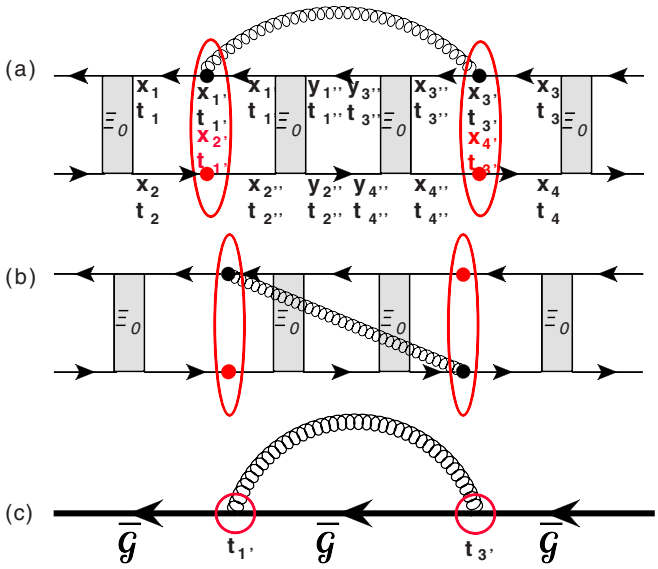

FIG. 2. (a) and (b) Prototypical first-order diagrams in $W^{\rm ph}$. Here arrows represent $\bar{G}$, the gray boxes are the SBSE kernel Ξ_0, and the wiggly lines stand for $W^{\rm ph}$. Red indicates inserts needed to express the result in terms of the two-times $\bar{\mathcal{G}}$ (see text). (c) Representation of the diagrams (a) and (b) in terms of $\bar{\mathcal{G}}$ (bold line).

diagrams of Fig. 2. Still we can make use of the following trick. The relation for the single-particle $\bar{G}$ [41],

$$\int dx_{2'}\, \bar{G}(x_{2'}t_{1'}2)\bar{G}(2''x_{2'}t_{1'}) = \pm i\bar{G}(2''2)\Theta(t_2t_{1'}t_{2''}) \qquad (11)$$

(with the + and − sign for hole and electron propagators, respectively), holds when $t_{1'}$ lies between t_2 and $t_{2''}$ as indicated by $\Theta(t_2t_{1'}t_{2''})$. In the Feynman diagrams of Figs. 2(a) and 2(b), using Eq. (11) corresponds to inserting additional space-spin points that are integrated over [red dots in Fig. 2(a)]. Their time coordinates can be chosen equal to an already existing time integration point, as indicated by the red ovals.

Taking $t_2 = t_1$ and $t_4 = t_3$, the Feynman diagram corresponds to the lesser part (i.e., $t_1 < t_3$) of the two-times two-particle correlation function (or exciton Green's function) $\mathcal{G}^<$. It is expressed in terms of two-times $\bar{\mathcal{G}}$ and $W^{\rm ph}$ [compare Figs. 2(a) and 2(b) with Fig. 2(c)]. The same applies to $\mathcal{G}^>$, when $t_1 > t_3$. On the basis of excitonic states where $\bar{\mathcal{G}}$ is diagonal, this reads

$$\mathcal{G}^<_{\lambda\lambda'}(t_{13}) = \bar{\mathcal{G}}^<_{\lambda\lambda}(t_{13})\delta_{\lambda\lambda'} + \int_{t_1}^{t_3} dt_{1'} \int_{t_{1'}}^{t_3} dt_{3'} \bar{\mathcal{G}}^<_{\lambda\lambda}(t_{11'})\Pi_{\lambda\lambda'}(t_{1'3'})\bar{\mathcal{G}}^<_{\lambda'\lambda'}(t_{3'3}), \qquad (12)$$

where t_{13} stands for (t_1, t_3), $\boldsymbol{\lambda} = (\lambda, \mathbf{q})$ labels the exciton band index λ and the exciton wave vector $\mathbf{q}$, and repeated indices are summed over. $\Pi_{\lambda\lambda'}(t_{13})$ given by

$$\Pi_{\lambda\lambda'}(t_{13}) = \sum_{\alpha} i\mathcal{W}^{\rm ph}_{\lambda\alpha\alpha\lambda'}(t_{13})\bar{\mathcal{G}}^<_{\alpha\alpha}(t_{13}) \qquad (13)$$

is an effective exciton self-energy, because $\bar{\mathcal{G}}_{\lambda\lambda}(t_{13})$ represents the propagator of independent excitons. It is the analog of the FM self-energy for one-particle excitations with $\bar{G}$ and $W^{\rm ph}$ replaced by $\bar{\mathcal{G}}$ and $\mathcal{W}^{\rm ph}$, respectively.

The effective exciton-exciton interaction $\mathcal{W}^{\rm ph}$ is given by matrix elements of $W^{\rm ph}$ that can be read from Fig. 2 and that are detailed in Appendix A. $\mathcal{W}^{\rm ph} = \mathcal{W}^{\rm ph}_{pp} + \mathcal{W}^{\rm ph}_{eh}$ consists of an effective electron-electron or hole-hole interaction labeled pp from the first diagram in Fig. 2(a), and an electron-hole (eh) interaction from the second diagram in Fig. 2(b). This reflects the fact that excitons are composite particles [47], and their effective interaction results from the interaction between their constituents, i.e., all electrons and holes. The two terms have opposite sign, leading to partial cancellation of dynamical effects as suggested in the case of dynamically screened Coulomb interaction [41,48].

In particular, writing $W^{\rm ph}$ in terms of the exciton propagator and el-ph matrix elements, the exciton self-energy in the frequency space at zero temperature takes the following expression:

$$\Pi_{\lambda\mathbf{q}\lambda'\mathbf{q}}(\omega) = \frac{1}{N}\sum_{\alpha\mu\bar{\mathbf{q}}} \frac{g^{\rm exc*}_{\alpha\lambda';\mu}(\mathbf{q},\bar{\mathbf{q}})g^{\rm exc}_{\alpha\lambda;\mu}(\mathbf{q},\bar{\mathbf{q}})}{\omega - (E_{\alpha\mathbf{q}+\bar{\mathbf{q}}} + \Omega_{\mu\bar{\mathbf{q}}}) + i\eta}, \qquad (14)$$

where $\Omega_{\mu\mathbf{q}}$ denotes the energy of the phonon with wave vector $\mathbf{q}$ and band index μ, $E_{\alpha\mathbf{q}}$ is the equivalent quantity for excitons, and $g^{\rm exc}_{\alpha\lambda;\mu}(\mathbf{q},\bar{\mathbf{q}})$ are the exciton-phonon matrix elements defined in Appendix A. Starting from the full dynamical BSE, we have provided a rigorous derivation of Eq. (14), which corresponds to a first-order expansion of the excitonic Hamiltonian in terms of $W^{\rm ph}$ [49–51]. This first-order expansion is based on the hypothesis, *a priori* unjustified, that dynamical effects induced by the el-ph interaction on neutral excitations can be described in terms of excitons coupled with phonons. Our derivation highlights the basic assumptions and approximations that justify its validity.

Finally, following the dynamical BSE scheme suggested in Ref. [52] in the context of dynamical effects induced by electronic correlation, a partial summation of Eq. (2) can be performed writing

$$\mathcal{G}^<_{\lambda\lambda'}(\omega) = \bar{\mathcal{G}}^<_{\lambda\lambda}(\omega) + \bar{\mathcal{G}}^<_{\lambda\lambda}(\omega)\Pi_{\lambda\alpha}(\omega)\mathcal{G}^<_{\alpha\lambda'}(\omega), \qquad (15)$$

where Π should be evaluated using $\mathcal{G}^<$ instead of $\bar{\mathcal{G}}^<$ in Eq. (13). This allows us to include a partial resummation of self-consistent contribution as well. Equation (15) represents a Dyson-like equation for the exciton propagator in the presence of the el-ph interaction that can be solved on top of a standard SBSE calculation of $\bar{\mathcal{G}}$. The relaxation of the TDA on the el-ph interaction does not have much of an effect on Eq. (15). Indeed, the inclusion of el-ph scattering processes between occupied and empty states gives rise to an additional static contribution to the exciton self-energy [51] that can be grouped together with the Debye-Waller term and included in the definition of $\bar{\mathcal{G}}$ (or $\bar{L}$).

At this point it is important to note that, although the Dyson equation with a first-order self-energy [as in Eq. (15)] can give in principle an accurate description of the QP properties such as QP energy and lifetime, it cannot capture the satellite physics. Indeed, several calculations of the one-particle G that solved a Dyson-like equation within GW [42,53–57] or HAC [8,9,29] approximations demonstrated that the position of the first satellite is wrong, and satellite replicas are

completely missed. On the other hand, satellite structures are well described through a cumulant approach [38,39,53–57]. In the following, we will provide a scheme that combines the two approaches (the Dyson equation and the cumulant representation) and allows us to treat QP and satellite features on the same footing.

First of all, following the idea of Bechstedt *et al.* [58] for the description of plasmonic satellites in the context of one-particle excitations, we cut the exciton self-energy in two parts: a QP contribution $\Pi_{\lambda\lambda}(E_\lambda^{\rm QP})$ evaluated at the exciton QP energy ($E_\lambda^{\rm QP}$) and a dynamical contribution $\Delta\Pi_{\lambda\lambda}(\omega) = \Pi_{\lambda\lambda}(\omega) - {\rm Re}\Pi_{\lambda\lambda}(E_\lambda^{\rm QP})$. Then we expand $\mathcal{G}$ at the first order in $\Delta\Pi$. Under these conditions, Eq. (15) becomes

$$\mathcal{G}^{\rm QP}_{\lambda\lambda}(\omega) = \bar{\mathcal{G}}_{\lambda\lambda}(\omega) + \bar{\mathcal{G}}_{\lambda\lambda}(\omega)\Pi_{\lambda\lambda}\big(E_\lambda^{\rm QP}\big)\mathcal{G}^{\rm QP}_{\lambda\lambda}(\omega), \quad (16)$$

$$\mathcal{G}_{\lambda\lambda}(\omega) = \mathcal{G}^{\rm QP}_{\lambda\lambda}(\omega) + \mathcal{G}^{\rm QP}_{\lambda\lambda}(\omega)\Delta\Pi_{\lambda\lambda}(\omega)\mathcal{G}^{\rm QP}_{\lambda\lambda}(\omega), \quad (17)$$

where $\mathcal{G}^{\rm QP}$ is the QP exciton propagator obtained replacing E_λ with $E_\lambda^{\rm QP}$ in the expression of $\bar{\mathcal{G}}$. The QP energy, according to Eq. (16), is obtained through the following self-consistent relation: $E_\lambda^{\rm QP} = E_\lambda + {\rm Re}\Pi_{\lambda\lambda}(E_\lambda^{\rm QP})$. Finally, from the comparison of Eq. (17) with the first-order expansion of a cumulant ansatz,

$$\mathcal{G}_{\lambda\lambda}(t_{13}) = \mathcal{G}^{\rm QP}_{\lambda\lambda}(t_{13})e^{C_\lambda(t_{13})} \approx \mathcal{G}^{\rm QP}_{\lambda\lambda}(t_{13})[1 + C_\lambda(t_{13})], \quad (18)$$

we obtain

$$C_\lambda(t_{13}) = -i\int_{t_1}^{t_3} dt_{1'}\int_{t_{1'}}^{t_3} dt_{3'}\,\Delta\Pi_{\lambda\lambda}(t_{1'3'})e^{iE_\lambda^{\rm QP}(t_{3'}-t_{1'})}. \quad (19)$$

The exciton propagator $\mathcal{G}_{\lambda\lambda}$ resulting from Eqs. (18) and (19) can be expressed in terms of a renormalization factor e^{-R_λ} describing the amount of spectral weight transferred from the QP to the satellite structures, the exciton linewidth Γ_λ induced by the el-ph coupling, and a term $\tilde{C}_\lambda$ responsible for satellite structures:

$$\mathcal{G}^{<}_{\lambda\lambda}(t_{13}) = e^{-R_\lambda}e^{-i(E_\lambda^{\rm QP}+i\Gamma_\lambda)(t_3-t_1)}e^{\tilde{C}_\lambda(t_{13})}, \quad (20)$$

where

$$R_\lambda = -\frac{\partial}{\partial\omega}\Pi_{\lambda\lambda}(\omega)|_{\omega=E_\lambda^{\rm QP}}, \quad (21)$$

$$\Gamma_\lambda = {\rm Im}\Pi_{\lambda\lambda}(\omega)|_{\omega=E_\lambda^{\rm QP}}, \quad (22)$$

$$\tilde{C}_\lambda(t_{13}) = -\frac{1}{\pi}\int_{-E_\lambda^{\rm QP}}^{+\infty} d\omega\,\frac{{\rm Im}\Pi_{\lambda\lambda}\big(\omega + E_\lambda^{\rm QP}\big)}{(\omega - i\eta)^2}e^{-i\omega(t_3-t_1)}. \quad (23)$$

The expression in Eq. (20) constitutes the main result of this work. Starting from basic equations in MBPT, it provides a clean derivation of the cumulant representation for the exciton Green's function in the presence of el-ph interaction. The approach allows us to include dynamical corrections induced by the el-ph interaction on both QP excitations and satellites in a systematic way, and it can be implemented as a postprocessing of standard SBSE calculations of the excitonic band structure and density functional perturbation theory (DFPT) calculations [59] of phonons and el-ph matrix elements. Actually, to be consistent with our theory, the el-ph interaction should be treated in the *GW* approximation [25,60–62], using, for example, the recently developed *GW* perturbation theory (GWPT) approach [63]. However, in standard semiconductors, correlation effects on the el-ph coupling beyond DFT are often negligible [64], and DFPT constitutes a good compromise.

In the next sections, we will apply this approach to a simple model system that will be used as an illustrative example to discuss the basic physical aspects of the cumulant in a general way.

IV. APPLICATION TO A SIMPLE MODEL SYSTEM

In the following, we will consider a model system consisting of two free-electron bands coupled with a nondispersive Einstein-like phonon of frequency Ω_0 living in a homogeneous medium of dielectric constants ϵ_0 and ϵ_∞. Moreover, we model the el-ph matrix elements $g_{n\mathbf{k},m\mathbf{k}+\mathbf{q}}$ describing electronic scattering processes from state ($n\mathbf{k}$) to state ($m\mathbf{k}+\mathbf{q}$) ($\mathbf{q}$ being the phonon wave vector) through the Fröhlich expression:

$$g_{\mathbf{q}} = \frac{i}{\mathbf{q}}\left[\frac{4\pi}{V}\frac{\Omega_0}{2}\left(\frac{1}{\epsilon_\infty} - \frac{1}{\epsilon_0}\right)\right]^{1/2}, \quad (24)$$

where V is the volume of the primitive cell. In this way, the el-ph matrix elements are independent from the electron wave vector $\mathbf{k}$ and the band index $n(m)$. Excitons, on the other hand, are described in the effective-mass approximation so that the solution of the SBSE are Wannier excitons with energy

$$E_{\lambda\mathbf{q}} = \Delta_{\rm QP} - \frac{\mu}{2\epsilon_\infty^2 n_\lambda^2} + \frac{q^2}{2M}, \quad (25)$$

where $\Delta_{\rm QP}$ is the QP band gap, μ is the reduced mass of the electron-hole pair, n_λ is the Rydberg quantum number of the state λ, M is the exciton mass, and q is the length of its wave vector. Under these conditions, the exciton self-energy in Eq. (14) evaluated at $\mathbf{q}\to\mathbf{0}$ takes the following expression (see Appendix B):

$$\Pi_{\lambda\lambda}(\omega) = \frac{4\alpha}{\pi}\frac{\sqrt{d}}{q_D}\Omega_0^2\int_0^{q_D} d\bar{q}\,\frac{1 - S_{\lambda\lambda}(\bar{q})}{\omega - (\Delta_{\rm QP} + \tilde{\Omega}_{\bar{q}}) + i\eta}, \quad (26)$$

where q_D is the Debye wave vector, $\tilde{\Omega}_q = \frac{q^2}{2M} + \Omega_0$, $\alpha = \sqrt{\frac{M}{2\Omega_0}}(\frac{1}{\epsilon_\infty} - \frac{1}{\epsilon_0})$ is the Fröhlich coupling constant for excitons, $d = \frac{q_D^2/2M}{\Omega_0}$ is the ratio between the exciton bandwidth inside the Debye sphere and the phonon frequency, and $S_{\lambda\lambda}(q)$ is the square modulus of the exciton envelop wave function that for the $1S$ state is $S(q) = \frac{1}{[1+(\frac{qa}{2})^2]^2}$ (a being the exciton Bohr radius). From the numerator of the integral in Eq. (26) we see that the exciton self-energy is the sum of the two opposite contributions which, as discussed in the previous section, are related to $\mathcal{W}^{\rm ph}_{pp}$ and $\mathcal{W}^{\rm ph}_{eh}$, respectively. The latter, in particular has a strong dependence from the Bohr radius through the factor $S_{\lambda\lambda}$. Inserting Eq. (26) in Eqs. (21)–(23) and using Eq. (19) we can evaluate the spectral function of $\mathcal{G}$ that, in the case of Wannier excitons, gives the absorption spectrum.

Figure 3(a) shows the SBSE and cumulant absorption spectra for the lowest excited state (Wannier exciton in the $1S$ configuration; we omit the subscript λ in the following). As pointed out by other approximate solutions of this model

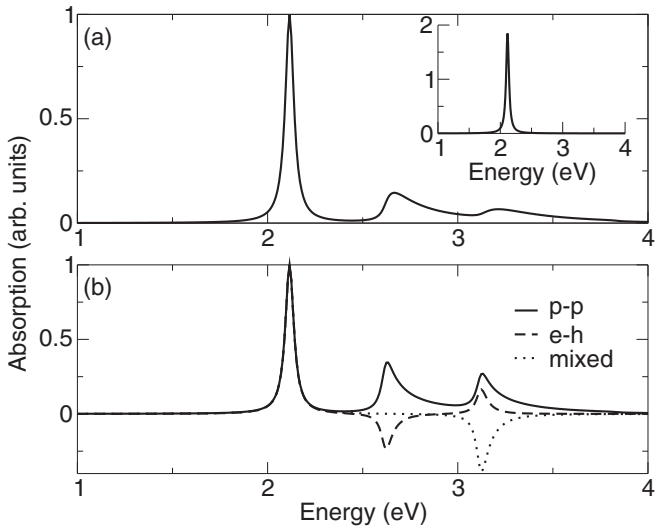

FIG. 3. Model absorption spectra renormalized to the strength of the QP peak. Main panels: cumulant results. (a) Total spectrum. (b) Comparison between the *pp*, *eh*, and mixed contributions. Inset in (a) Absorption spectrum from the SBSE, with a broadening of 0.03 eV.

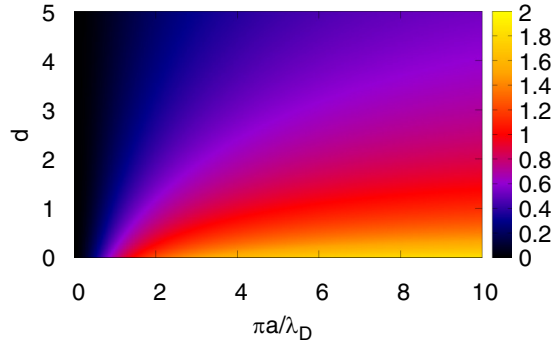

FIG. 4. Intensity plot of the rescaled renormalization factor $R/\frac{2\alpha\sqrt{d}}{\pi}$. On the horizontal axis, the exciton Bohr radius renormalized with the Debye wavelength λ_D. On the vertical axis, the ratio d between the exciton bandwidth and the phonon frequency.

system based on perturbation theory [65] and variational method [66], the coupling with phonons creates a series of satellites at energies $E + n\Omega_0$ with integer n, and a weight transfer from the QP peak to the satellites, due to e^{-R}.

Figure 3(b) highlights *pp*, *eh*, and (for the second satellite) mixed contributions. In the first satellite, the *pp* and *eh* terms have opposite sign, but the negative *eh* contributions are always smaller. Since the resulting structures are located at the same frequency, the spectral function remains positive. The strength of the second satellite goes as $[\mathcal{W}^{\rm ph}]^2$ according to an expansion of Eq. (18). Therefore, only the mixed contribution stemming from the product *pp*-*eh* is negative.

In the following, to better understand how dynamical effects related to the coupling with phonons are related to the properties of the system, we will focus on the behavior of the renormalization factor R. It describes the amount of spectral weight transferred from the QP peak to the satellite structures. Moreover, it measures how relevant the exciton-phonon coupling is: a larger R corresponds to a more important exciton-phonon coupling. According to the structure of $\mathcal{W}^{\rm ph}$, it is convenient to separate the renormalization factor in *pp* and *eh* contributions: $R = R_{pp} + R_{eh}$ with

$$R_{pp} = \frac{2\alpha\sqrt{d}}{\pi}\left[\frac{1}{1+d} + \frac{\arctan\sqrt{d}}{\sqrt{d}}\right], \tag{27}$$

$$R_{eh} = \frac{2\alpha\sqrt{d}}{\pi}\left[\left(\frac{d}{(\pi a/\lambda_D)^2}\right)^2 \frac{2}{\sqrt{d}} f\left(d, \frac{\pi a}{\lambda_D}\right)\right]. \tag{28}$$

Here $\lambda_D = \frac{2\pi}{q_D}$ is the Debye wavelength and f is a dimensionless function defined by the integral

$$f\left(d, \frac{\pi a}{\lambda_D}\right) = \int_0^{\sqrt{d}} \frac{dx}{\left[\left(\frac{d}{(\pi a/\lambda_D)^2} + x^2\right)(1+x^2)\right]^2}. \tag{29}$$

From Eq. (27) we see that R_{pp} is an implicit function of the exciton mass M through the quantity d inside the expression in the square brackets. The prefactor is a dimensionless constant since the M dependence in $\sqrt{d}$ is exactly canceled by the Fröhlich coupling constant α. The *eh* contribution [see Eq. (28)], on the other hand, is also a function of the exciton Bohr radius through the quantity $\frac{\pi a}{\lambda_D}$.

Figure 4 shows the behavior of the rescaled renormalization factor $R/(\frac{2\alpha\sqrt{d}}{\pi})$ as a function of d and $\pi a/\lambda_D$. The weight transfer is important for nondispersive excitons (small d), and much weaker when $d \gg 1$. Indeed, the exciton bandwidth is related to the rate of the exciton hopping processes, while the phonon frequency Ω_0 expresses the time scale of the lattice dynamics of the system. When $d \gg 1$, the hopping processes are fast compared to the lattice vibrations and the exciton behaves like a particle propagating in a frozen lattice, so $W^{\rm ph}$ is negligible. For fixed d, the evolution of R with $\pi a/\lambda_D$ shows that a strongly localized exciton is much less influenced by dynamical effects. This can be attributed to the fact that R is a sum of *pp* and *eh* contributions, with R_{pp} positive and independent of a and R_{eh} negative and vanishing for $\frac{\pi a}{\lambda_D} \to \infty$ (see Fig. 5). Therefore, R_{pp} and R_{eh} cancel to a large extent for small a. In particular, as can be inferred from Fig. 5, the cancellation becomes exact for $\frac{\pi a}{\lambda_D} \to 0$.

The different behavior of R_{pp} and R_{eh} is strictly related to the different length scale of $\mathcal{W}^{\rm ph}_{pp}$ and $\mathcal{W}^{\rm ph}_{eh}$ that defines the distance to which two particles (electrons or holes) and an electron-hole pair interact through a phonon exchange. Indeed, while the length scale of $\mathcal{W}^{\rm ph}_{pp}$ is set by λ_D, due to the excitonic effects, the length scale for $\mathcal{W}^{\rm ph}_{eh}$ is of the order of $\sqrt{a^2 + \lambda_D^2}$. This explains why $|\mathcal{W}^{\rm ph}_{eh}| < |\mathcal{W}^{\rm ph}_{pp}|$ for each a. For $a \gg \lambda_D$ the *e*-*h* distance is proportional to a, independently of λ_D, such that $|\mathcal{W}^{\rm ph}_{eh}|$ becomes negligible. When $a \ll \lambda_D$ the typical length scale is λ_D, the same for $\mathcal{W}^{\rm ph}_{pp}$ and $\mathcal{W}^{\rm ph}_{eh}$, and the cancellation becomes exact. In real systems, the different character of the valence and conduction states can make the cancellation imperfect, but this will not change the trends. Indeed, the exact cancellation for $a \ll \lambda_D$ persists in the long-range part of the exciton-phonon interaction, which is the only one considered in the Fröhlich model.

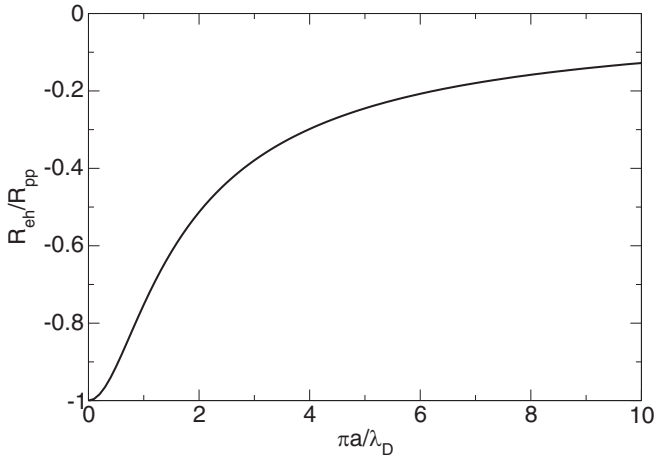

FIG. 5. Behavior of the ratio between *eh* and *pp* contributions to the renormalization factor as a function of the rescaled exciton Bohr radius.

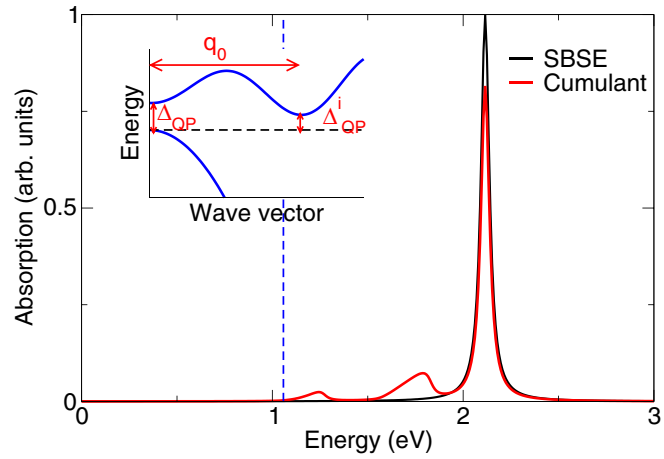

FIG. 6. Main panel: model absorption spectra renormalized to the strength of the SBSE main peak. The blue dashed line indicates the position of the indirect QP gap Δ^i_{QP}. Inset: schematic electronic band structure of an indirect-band-gap semiconductor. In our model, the conduction band is described in terms of two valleys with the same electronic mass.

From this analysis we can conclude that dynamical effects induced by the coupling with phonons are the result of a delicate competition between several effects related to the electronic localization. Indeed, localization reduces the screening efficiency increasing the strength of the electron-phonon interaction that in the present model is described by the Fröhlich coupling constant α. At the same time, it gives rise to weakly dispersive excitons corresponding to a small exciton bandwidth. Both effects would enhance the exciton-phonon coupling. However, electronic localization results in a small exciton Bohr radius that causes cancellation effects.

Finally, inserting the expression of the exciton self-energy Eq. (26) into Eq. (22), we can evaluate the exciton linewidth that for the $1S$ exciton at wave vector $\mathbf{q}$ is

$$\Gamma_{\mathbf{q}} = \frac{2\alpha\Omega_0}{\sqrt{d_{\mathbf{q}}-1}}\left[1-\frac{1}{\left[1+\left(1-\frac{1}{d_{\mathbf{q}}}\right)\left(\frac{aq}{2}\right)^2\right]^2}\right]\theta(d_{\mathbf{q}}-1), \tag{30}$$

where we have introduced the quantity $d_{\mathbf{q}} = \frac{q^2/2M}{\Omega_0}$. As we can see from Eq. (30), the exciton takes a finite lifetime only for energy values larger than Ω_0. This is intuitive since at zero temperature, when only phonon emission processes are involved, decay channels below the phonon frequency are not allowed by energy conservation. This is consistent with the fact that the lowest excited state of any many-body system should have infinite lifetime at zero temperature. We emphasize that the only inclusion of the FM self-energy in the one-particle Green's function would give a completely different result. Indeed, in this case the lowest excited state of a direct-gap semiconductor is undamped only when excitonic effects are neglected (i.e., in an independent-particle picture). The inclusion of the electron-hole interaction causes a mixing of the lowest energy undamped electron-hole pair associated to the QP gap with higher-energy damped excitations that always results in the formation of a damped exciton independently of its energy. This nonphysical behavior is directly related to the lack of the class of diagrams shown in Fig. 1(d).

V. PHONON-ASSISTED ABSORPTION IN THE CUMULANT SCHEME

In this section, we will show how the cumulant approach allows one to describe phonon-assisted absorption in terms of satellites in the optical spectra induced by the exciton-phonon coupling. To this end, we generalize the previous model to a two-band system displayed in the inset of Fig. 6. The lowest excited states of this prototypical indirect-gap semiconductor can be classified in terms of direct and indirect Wannier excitons. The latter are described by the same equations used for the direct exciton with the exciton wave vector $\mathbf{q}$ replaced by $\mathbf{q}-\mathbf{q}_0$ ($\mathbf{q}_0$ being the distance between the two conduction-band minima). As a consequence, the energy of an indirect exciton with wave vector $\mathbf{q}$ in the Rydberg state λ is

$$E_{\lambda\mathbf{q}} = \Delta^i_{\mathrm{QP}} - \frac{\mu}{2\epsilon_\infty^2 n_\lambda^2} + \frac{|\mathbf{q}-\mathbf{q}_0|^2}{2M}, \tag{31}$$

where Δ^i_{QP} is the indirect QP gap. The same applies to the exciton envelope wave function. In analogy with the direct-gap semiconductor discussed in the previous section, the optical spectrum is determined only by direct excitons. However, their self-energy, beside a sum over direct excitons, also involves indirect transitions with smaller energies.

For simplicity, in the following we consider only contribution to the self-energy coming from the indirect transitions. Moreover, we make the assumptions that the two conduction-band minima have the same curvature, q_0 is similar to q_D, and $d \gg 1$. These are essential requirements for the validity of the effective-mass approximation for both direct and indirect transitions. Under these conditions, the exciton self-energy becomes (see Appendix B)

$$\Pi_{\lambda\lambda}(\omega) = \frac{2\alpha}{\pi}\frac{\sqrt{d_c}}{q_c}\Omega_0^2\int_0^{q_c} d\bar{q}\, f(\bar{q})\frac{1-S_{\lambda\lambda}(\bar{q})}{\omega-\left(\Delta^i_{\mathrm{QP}}+\tilde{\Omega}_{\bar{q}}\right)+i\eta}, \tag{32}$$

where $q_c = q_D - q_0$, $d_c = \frac{q_c^2/2M}{\Omega_0}$, and $f(q) = \frac{\bar{q}}{q_0} \ln|\frac{\bar{q}+q_0}{\bar{q}-q_0}|$. Inserting Eq. (32) into Eqs. (21) and (23), we can evaluate the optical absorption spectrum.

In Fig. 6 we compare the optical spectra of our two band model system evaluated within SBSE and the cumulant approximations. Also in this case the exciton-phonon interaction gives rise to new features in the spectrum. In particular, the first peak below the main direct exciton peak is located at energy $\Delta^i_{\mathrm{QP}} + \Omega_0$. It is associated with elementary scattering processes between direct and indirect excitons through phonon exchange as expected in phonon assisted processes. The other feature, as expected is a satellite replica related to multi phonon processes.

VI. CONCLUSIONS

In conclusion, starting from basic equations of MBPT, we have derived a cumulant formulation for neutral excitation spectra that contains excitonic effects and the coupling between excitons and phonons. The cumulant approach allows us to include dynamical effects arising from the el-ph coupling in a simple and intuitive way. It can be implemented as a post-processing of a standard GW+BSE calculation of excitonic states and a DFPT calculation of phonons and el-ph coupling. We demonstrate that, in order to obtain a consistent treatment of exciton-phonon coupling, diagrams have to be taken into account that can be neglected when the effect of lattice vibrations is treated in a static or quasistatic approximation. From the application of this approach to a model system, we analyzed the main features of the exciton-phonon coupling and provided a general picture of their link with the properties of materials such as exciton mass and exciton Bohr radius.

ACKNOWLEDGMENTS

This research was supported by the IRP funding of uni.lu/University of Luxembourg (project SOCMAT).

APPENDIX A: EXPLICIT EXPRESSION OF THE EXCITON-PHONON COUPLING

The particle-particle and electron-hole contributions to the effective exciton-exciton interaction $\mathcal{W}^{\mathrm{ph}}$ in Eq. (13) of the main text can be directly read from the diagrams in Fig. 2. In the basis of the excitonic eigenstates ($A^{vc\mathbf{k}}_{\lambda\mathbf{q}}$) where the solution $\bar{\mathcal{G}}$ of the SBSE is diagonal, this yields

$$
\begin{aligned}
&\mathcal{W}^{pp}_{\lambda\mathbf{q}\alpha\mathbf{q}'\alpha\mathbf{q}'\lambda'\mathbf{q}}(t_{1'3'}) \\
&= \sum_{v_1c_1v_2c_2\bar{v}_1\bar{v}_2} \sum_{\mathbf{k}_1\mathbf{k}_2} A^{v_1c_1\mathbf{k}_1 *}_{\lambda\mathbf{q}} A^{\bar{v}_2c_2\mathbf{k}_2 *}_{\alpha\mathbf{q}'} W^{v_1\mathbf{k}_1+\mathbf{q}v_2\mathbf{k}_2+\mathbf{q}}_{\bar{v}_2\mathbf{k}_2+\mathbf{q}'\bar{v}_1\mathbf{k}_1+\mathbf{q}'}(t_{1'3'}) A^{\bar{v}_1c_1\mathbf{k}_1}_{\alpha\mathbf{q}'} A^{v_2c_2\mathbf{k}_2}_{\lambda'\mathbf{q}} \\
&\quad + \sum_{v_1c_1v_2c_2\bar{c}_1\bar{c}_2} \sum_{\mathbf{k}_1\mathbf{k}_2} A^{v_1c_1\mathbf{k}_1 *}_{\lambda\mathbf{q}} A^{v_2\bar{c}_2\mathbf{k}_2+\mathbf{q}-\mathbf{q}' *}_{\alpha\mathbf{q}'} W^{c_2\mathbf{k}_2c_1\mathbf{k}_1}_{\bar{c}_1\mathbf{k}_1+\mathbf{q}-\mathbf{q}'\bar{c}_2\mathbf{k}_2+\mathbf{q}-\mathbf{q}'}(t_{3'1'}) A^{v_1\bar{c}_1\mathbf{k}_1+\mathbf{q}-\mathbf{q}'}_{\alpha\mathbf{q}'} A^{v_2c_2\mathbf{k}_2}_{\lambda'\mathbf{q}} \\
&\mathcal{W}^{eh}_{\lambda\mathbf{q}\alpha\mathbf{q}'\alpha\mathbf{q}'\lambda'\mathbf{q}}(t_{1'3'}) \\
&= - \sum_{v_1c_1v_2c_2\bar{v}\bar{c}} \sum_{\mathbf{k}_1\mathbf{k}_2} A^{v_1c_1\mathbf{k}_1 *}_{\lambda\mathbf{q}} A^{v_2\bar{c}\mathbf{k}_2+\mathbf{q}-\mathbf{q}' *}_{\alpha\mathbf{q}'} W^{v_1\mathbf{k}_1+\mathbf{q}\bar{c}\mathbf{k}_2+\mathbf{q}-\mathbf{q}'}_{c_2\mathbf{k}_2\bar{v}\mathbf{k}_1+\mathbf{q}'}(t_{1'3'}) A^{\bar{v}c_1\mathbf{k}_1}_{\alpha\mathbf{q}'} A^{v_2c_2\mathbf{k}_2}_{\lambda'\mathbf{q}} \\
&\quad - \sum_{v_1c_1v_2c_2\bar{v}\bar{c}} \sum_{\mathbf{k}_1\mathbf{k}_2} A^{v_1c_1\mathbf{k}_1 *}_{\lambda\mathbf{q}} A^{\bar{v}c_2\mathbf{k}_2 *}_{\alpha\mathbf{q}'} W^{\bar{v}\mathbf{k}_2+\mathbf{q}'c_1\mathbf{k}_1}_{\bar{c}\mathbf{k}_1+\mathbf{q}-\mathbf{q}'v_2\mathbf{k}_2+\mathbf{q}}(t_{3'1'}) A^{v_1\bar{c}\mathbf{k}_1+\mathbf{q}-\mathbf{q}'}_{\alpha\mathbf{q}'} A^{v_2c_2\mathbf{k}_2}_{\lambda'\mathbf{q}},
\end{aligned}
\tag{A1}
$$

where matrix elements $W^{\mathbf{ij}}_{\mathbf{lm}}$ of W^{ph} are defined in terms of single-particle wave functions ϕ as

$$
W^{\mathbf{ij}}_{\mathbf{lm}}(t_{12}) = \int d\mathbf{r}_{12} \phi^*_{\mathbf{i}}(\mathbf{r}_1) \phi^*_{\mathbf{l}}(\mathbf{r}_2) W^{\mathrm{ph}}(12) \phi_{\mathbf{j}}(\mathbf{r}_2) \phi_{\mathbf{m}}(\mathbf{r}_1), \tag{A2}
$$

and v (c) stands for valence (conduction) states.

Expressing W^{ph} in terms of the el-ph coupling and phonon propagator, Eq. (A2) becomes

$$
W^{i\mathbf{k}_i j\mathbf{k}_j}_{l\mathbf{k}_l m\mathbf{k}_m}(t_{12}) = \frac{1}{N} \sum_{\mu\mathbf{q}} g^*_{mi,\mu}(\mathbf{k}_i, \mathbf{q}) D_{\mu\mathbf{q}}(t_{12}) g_{lj,\mu}(\mathbf{k}_j, \mathbf{q}) \delta_{\mathbf{k}_m,\mathbf{k}_i+\mathbf{q}} \delta_{\mathbf{k}_l,\mathbf{k}_j+\mathbf{q}}. \tag{A3}
$$

Inserting Eqs. (A3) and (A1) into Eq. (13) and taking the Fourier transform, we obtain the expression in Eq. (14) with the following definition of the exciton-phonon matrix elements:

$$
g^{\mathrm{exc}}_{\alpha\lambda,\mu}(\mathbf{q}, \bar{\mathbf{q}}) = \sum_{v\bar{v}c\mathbf{k}} A^{vc\mathbf{k}}_{\lambda\mathbf{q}} g_{\bar{v}v,\mu}(\mathbf{k}+\mathbf{q}, \bar{\mathbf{q}}) A^{\bar{v}c\mathbf{k}*}_{\alpha\mathbf{q}+\bar{\mathbf{q}}} - \sum_{c\bar{c}v\mathbf{k}} A^{vc\mathbf{k}}_{\lambda\mathbf{q}} g^*_{\bar{c}c,\mu}(\mathbf{k}, \bar{\mathbf{q}}) A^{v\bar{c}\mathbf{k}+\bar{\mathbf{q}}*}_{\alpha\mathbf{q}-\bar{\mathbf{q}}}. \tag{A4}
$$

APPENDIX B: WANNIER EXCITON COUPLED WITH EINSTEIN PHONON

In this Appendix, we give details concerning the model system consisting of a Wannier exciton coupled with an Einstein phonon of frequency Ω_0 through a Fröhlich-like interaction. In the case of a Wannier exciton, the excitonic state $A^{vc\mathbf{k}}_{\lambda\mathbf{q}}$ is directly related to the envelope exciton wave function $F_\lambda(\mathbf{r})$ (solution of the hydrogenlike Hamiltonian describing the relative motion of

the electron-hole pairs in the Wannier model). In particular, $A^{vc\mathbf{k}}_{\lambda\mathbf{q}} = F_\lambda(\mathbf{k}+\gamma\mathbf{q})$, where $F_\lambda(\mathbf{k})$ is the Fourier transform of $F_\lambda(\mathbf{r})$ and $\gamma = \frac{m_c}{m_c+m_v}$ (m_v and m_c being the mass of the hole and the electron, respectively). The phonon propagator is $\mathbf{q}$-independent and is given by the following expression:

$$D(t_{12}) = -i[\theta(t_2-t_1)e^{-i\Omega_0(t_3-t_1)} + \theta(t_1-t_2)e^{i\Omega_0(t_3-t_1)}]. \tag{B1}$$

Thus using Eqs. (B1) into Eq. (A1), we obtain

$$\begin{aligned}\mathcal{W}^{\mathrm{ph}}_{\lambda\mathbf{q}\alpha\mathbf{q}'\alpha\mathbf{q}'\lambda'\mathbf{q}}(t_{12}) = |g_{\mathbf{q}'}|^2\Bigg[&D(t_{12})\sum_{\mathbf{k}}F^*_\lambda(\mathbf{k}+\gamma\mathbf{q})F_\alpha[-\mathbf{k}-\gamma(\mathbf{q}'+\mathbf{q})]\sum_{\mathbf{k}}F_{\lambda'}(\mathbf{k}+\gamma\mathbf{q})F^*_\alpha[-\gamma(\mathbf{q}+\mathbf{q}')-\mathbf{k}]\\
&+D(t_{21})\sum_{\mathbf{k}}F^*_\lambda(\mathbf{k}+\gamma\mathbf{q})F_\alpha[-\gamma(\mathbf{q}+\mathbf{q}')+\mathbf{q}'-\mathbf{k}]\sum_{\mathbf{k}}F_{\lambda'}(\mathbf{k}+\gamma\mathbf{q})F^*_\alpha[-\gamma(\mathbf{q}+\mathbf{q}')+\mathbf{q}'-\mathbf{k}]\\
&-D(t_{12})\sum_{\mathbf{k}}F^*_\lambda(\mathbf{k}+\gamma\mathbf{q})F_\alpha[-\gamma(\mathbf{q}+\mathbf{q}')+\mathbf{q}'-\mathbf{k}]\sum_{\mathbf{k}}F_{\lambda'}(\mathbf{k}+\gamma\mathbf{q})F^*_\alpha[(-\gamma)(\mathbf{q}+\mathbf{q}')-\mathbf{k}]\\
&-D(t_{21})\sum_{\mathbf{k}}F^*_\lambda(\mathbf{k}+\gamma\mathbf{q})F_\alpha[-\gamma(\mathbf{q}+\mathbf{q}')-\mathbf{k}]\sum_{\mathbf{k}}F_{\lambda'}(\mathbf{k}+\gamma\mathbf{q})F^*_\alpha[-\gamma(\mathbf{q}+\mathbf{q}')+\mathbf{q}'-\mathbf{k}]\Bigg],\end{aligned} \tag{B2}$$

where $g_{\mathbf{q}}$ is defined in Eq. (24). Alternatively, inserting $g_{\mathbf{q}}$ and $F_\lambda(\mathbf{k}+\gamma\mathbf{q})$ in Eq. (A4) we can express $\mathcal{W}^{\mathrm{ph}}$ in terms of the exciton-phonon matrix elements that in the present model have an analytical expression in terms of the electron and hole mass and the exciton Bohr radius [67–69].

For an exciton at $\mathbf{q}=\mathbf{0}$ in the state λ, this gives the self-energy:

$$\begin{aligned}\Pi_{\lambda\lambda}(t_{13}) = -\frac{i}{N}\sum_{\alpha\mathbf{q}'}|g_{\mathbf{q}'}|^2 e^{-i(E_{\alpha\mathbf{q}'}+\Omega_0)(t_3-t_1)}\Bigg[&\int d\mathbf{r}_{12}F^*_\lambda(\mathbf{r}_1)F_\alpha(\mathbf{r}_1)F^*_\alpha(\mathbf{r}_2)F_\lambda(\mathbf{r}_2)e^{-i\gamma\mathbf{q}'\cdot(\mathbf{r}_2-\mathbf{r}_1)}\\
&+\int d\mathbf{r}_{12}F^*_\lambda(\mathbf{r}_1)F_\alpha(\mathbf{r}_1)F^*_\alpha(\mathbf{r}_2)F_\lambda(\mathbf{r}_2)e^{-i(\gamma-1)\mathbf{q}'\cdot(\mathbf{r}_2-\mathbf{r}_1)} - \int d\mathbf{r}_{12}F^*_\lambda(\mathbf{r}_1)F_\alpha(\mathbf{r}_1)F^*_\alpha(\mathbf{r}_2)F_\lambda(\mathbf{r}_2)e^{i\mathbf{q}'\cdot\mathbf{r}_2}e^{-i\gamma\mathbf{q}'\cdot(\mathbf{r}_2-\mathbf{r}_1)}\\
&-\int d\mathbf{r}_{12}F^*_\lambda(\mathbf{r}_1)F_\alpha(\mathbf{r}_1)F^*_\alpha(\mathbf{r}_2)F_\lambda(\mathbf{r}_2)e^{-i\mathbf{q}'\cdot\mathbf{r}_1}e^{-i\gamma\mathbf{q}'\cdot(\mathbf{r}_2-\mathbf{r}_1)}\Bigg]\end{aligned} \tag{B3}$$

with

$$E_{\alpha\mathbf{q}} = \Delta_{\mathrm{QP}} - \frac{\mu}{2\epsilon^2_\infty n^2_\alpha} + \frac{q^2}{2M}, \tag{B4}$$

where Δ_{QP} is the QP band gap, μ is the reduced mass of the electron-hole pair, n_α is the Rydberg quantum number associated with the state α, $M = m_v + m_c$ is the mass of the exciton, and q is the length of its wave vector.

Since a typical Wannier exciton is characterized by a binding energy of two orders of magnitude smaller than the quasiparticle gap, in the sum over α we can neglect the quantity $\frac{\mu}{2\epsilon^2 n^2_\alpha}$. Thus, we can make the approximation

$$\sum_\alpha F^*_\alpha(\mathbf{r}_1)F^*_\alpha(\mathbf{r}_2)e^{-iE_{\alpha\mathbf{q}'}(t_3-t_1)} \approx \delta(\mathbf{r}_1-\mathbf{r}_2)e^{-i(\Delta_{\mathrm{QP}}+\frac{q'^2}{2M})(t_3-t_1)} \tag{B5}$$

that corresponds to include in the sum over α only free electron-hole states. This approximation is exact for $m_v = m_c$, when the contribution coming from bound electron-hole states is zero [69]. Under these conditions, we have

$$\Pi_{\lambda\lambda}(t_{13}) = -\frac{i}{2\pi^2}\Omega_0\left(\frac{1}{\epsilon_\infty}-\frac{1}{\epsilon_0}\right)\int d\mathbf{q}'\frac{1}{|\mathbf{q}'|^2}[1-S_{\lambda\lambda}(\mathbf{q}')]e^{-i(\Delta_{\mathrm{QP}}+\tilde{\Omega}_{\mathbf{q}})(t_3-t_1)}, \tag{B6}$$

where the integral over $\mathbf{q}'$ is performed inside the Debye sphere, and the first and second terms refer to the contribution coming from $\mathcal{W}^{pp}$ and $\mathcal{W}^{eh}$, respectively. $\tilde{\Omega}_{\mathbf{q}} = \frac{q^2}{2M} + \Omega_0$, and the function $S_{\lambda\lambda}$ that appears in the electron-hole contribution to the effective exciton-exciton interaction is defined as

$$S_{\lambda\lambda}(\mathbf{q}) = \int d\mathbf{r}|F_\lambda(\mathbf{r})|^2 e^{i\mathbf{q}'\mathbf{r}}. \tag{B7}$$

For the lowest exciton, $S_{\lambda\lambda}(\mathbf{q}) = \frac{1}{[1+\frac{q^2a^2}{4}]^2}$, where a is the exciton Bohr radius.

In the case of the indirect-gap semiconductor, the sum over α in Eq. (B3) runs over the indirect excitonic states for which

$$E_{\alpha\mathbf{q}} = \Delta^i_{\mathrm{QP}} - \frac{\mu}{2\epsilon_0 n_\alpha} + \frac{|\mathbf{q}-\mathbf{q}_0|^2}{2M} \tag{B8}$$

and $A^{vc\mathbf{k}}_{\alpha\mathbf{q}} = F_\alpha[\mathbf{k} + \gamma(\mathbf{q} - \mathbf{q}_0)]$. This leads to the following expression for the exciton self-energy:

$$\Pi_{\lambda\lambda}(t_{13}) = -\frac{i}{2\pi^2}\Omega_0\left(\frac{1}{\epsilon_\infty} - \frac{1}{\epsilon_0}\right)\int_{S_0} d\mathbf{q}' \frac{1}{|\mathbf{q}' + \mathbf{q}_0|^2}[1 - S_{\lambda\lambda}(\mathbf{q}')]e^{-i(\Delta^i_{\mathrm{QP}} + \tilde{\Omega}_{\mathbf{q}})(t_3 - t_1)}, \tag{B9}$$

where S_0 denotes a sphere of radius $q_D - q_0$ centered in $\mathbf{q}_0$, and λ labels the lowest-energy direct Wannier exciton.

[1] F. Giustino, Rev. Mod. Phys. **89**, 015003 (2017).
[2] F. Bassani and G. P. Parravicini, *Electronic States and Optical Transitions in Solids* (Pergamon, Oxford, 1975).
[3] L. Hall, J. Bardeen, and F. Blatt, Phys. Rev. **95**, 559 (1954).
[4] F. Paleari, H. P. C. Miranda, A. Molina-Sánchez, and L. Wirtz, Phys. Rev. Lett. **122**, 187401 (2019).
[5] E. Cannuccia, B. Monserrat, and C. Attaccalite, Phys. Rev. B **99**, 081109(R) (2019).
[6] P. M. Chaikin, A. F. Garito, and A. J. Heeger, Phys. Rev. B **5**, 4966 (1972).
[7] M. Nirmal *et al.*, Z. Phys. D **26**, 361 (1993).
[8] S. Moser *et al.*, Phys. Rev. Lett. **110**, 196403 (2013).
[9] C. Cancellieri, A. S. Mishchenko, U. Aschauer, A. Filippetti, C. Faber, O. S. Barišić, V. A. Rogalev, T. Schmitt, N. Nagaosa, and V. N. Strocov, Nat. Commun. **7**, 10386 (2016).
[10] D. Emin, *Polarons* (Cambridge University Press, Cambridge, England, 2013).
[11] G. Grimvall, *The Electron-phonon Interaction in Metals* (North-Holland, Amsterdam, 1981).
[12] J. R. Schrieffer, *Theory of Superconductivity*, Advanced Book Program Series (Perseus, 1983).
[13] G. D. Mahan, *Many-Particle Physics*, 2nd ed. (Plenum, New York, 1993).
[14] A. S. Alexandrov and J. T. Devreese, *Advances in Polaron Physics* (Springer, New York, 2010).
[15] T. Feldtmann, M. Kira, and S. W. Koch, Phys. Status Solidi B **246**, 332 (2009).
[16] R. Martin, L. Reining, and D. Ceperley, *Interacting Electrons: Theory and Computational Approaches* (Cambridge University Press, Cambridge, 2016).
[17] A. L. Fetter and J. D. Walecka, *Quantum Theory of Many-Particle Systems* (McGraw-Hill, Mineola, New York, 1971).
[18] G. Strinati, Riv. Nuovo Cimento **11**, 1 (1988).
[19] G. Onida, L. Reining, and A. Rubio, Rev. Mod. Phys. **74**, 601 (2002).
[20] P. B. Allen and V. Heine, J. Phys. C **9**, 2305 (1976).
[21] P. B. Allen and M. Cardona, Phys. Rev. B **23**, 1495 (1981).
[22] F. Giustino, S. G. Louie, and M. L. Cohen, Phys. Rev. Lett. **105**, 265501 (2010).
[23] E. Cannuccia and A. Marini, Phys. Rev. Lett. **107**, 255501 (2011).
[24] E. Cannuccia and A. Marini, Eur. Phys. J. B **85**, 320 (2012).
[25] G. Antonius, S. Poncé, P. Boulanger, M. Côté, and X. Gonze, Phys. Rev. Lett. **112**, 215501 (2014).
[26] H. Kawai, K. Yamashita, E. Cannuccia, and A. Marini, Phys. Rev. B **89**, 085202 (2014).
[27] S. Poncé, Y. Gillet, J. L. Janssen, A. Marini, M. Verstraete, and X. Gonze, J. Chem. Phys. **143**, 102813 (2015).
[28] A. Marini, Phys. Rev. Lett. **101**, 106405 (2008).
[29] C. Chen, J. Avila, E. Frantzeskakis, A. Levy, and M. C. Asensio, Nat. Commun. **6**, 8585 (2015).
[30] G. Antonius, S. Poncé, E. Lantagne-Hurtubise, G. Auclair, X. Gonze, and M. Côté, Phys. Rev. B **92**, 085137 (2015).
[31] G. Strinati, Phys. Rev. Lett. **49**, 1519 (1982).
[32] G. Strinati, Phys. Rev. B **29**, 5718 (1984).
[33] L. Hedin, J. Phys.: Condens. Matter **11**, R489 (1999).
[34] D. C. Langreth, Phys. Rev. B **1**, 471 (1970).
[35] O. Gunnarsson, V. Meden, and K. Schonhammer, Phys. Rev. B **50**, 10462 (1994).
[36] J. S. Zhou, J. J. Kas, L. Sponza, I. Reshetnyak, M. Guzzo, C. Giorgetti, M. Gatti, F. Sottile, J. J. Rehr, and L. Reining, J. Chem. Phys. **143**, 184109 (2015).
[37] S. M. Story, J. J. Kas, F. D. Vila, M. J. Verstraete, and J. J. Rehr, Phys. Rev. B **90**, 195135 (2014).
[38] C. Verdi, F. Caruso, and F. Giustino, Nat. Commun. **8**, 15769 (2017).
[39] F. Caruso, C. Verdi, S. Poncé, and F. Giustino, Phys. Rev. B **97**, 165113 (2018).
[40] J. P. Nery, P. B. Allen, G. Antonius, L. Reining, A. Miglio, and X. Gonze, Phys. Rev. B **97**, 115145 (2018).
[41] P. Cudazzo and L. Reining, Phys. Rev. Research **2**, 012032(R) (2020).
[42] F. Aryasetiawan, L. Hedin, and K. Karlsson, Phys. Rev. Lett. **77**, 2268 (1996).
[43] L. Hedin, Phys. Rev. **139**, A796 (1965).
[44] K. Shindo, J. Phys. Soc. Jpn. **29**, 287 (1970).
[45] I. Tamm, J. Phys. (USSR) **9**, 449 (1945).
[46] S. M. Dancoff, Phys. Rev. **78**, 382 (1950).
[47] M. Combescot and S.-Y. Shiau, *Excitons and Cooper Pairs: Two Composite Bosons in Many-Body Physics* (Oxford Graduate Texts, Oxford, 2015).
[48] F. Bechstedt, K. Tenelsen, B. Adolph, and R. Del Sole, Phys. Rev. Lett. **78**, 1528 (1997).
[49] A. S. Davydov, *Theory of Molecular Excitons* (Springer, New York, 1971).
[50] W. Bardyszewski, M. Prywata, and D. Yevick, J. Appl. Phys. **90**, 222 (2001).
[51] G. Antonius and S. G. Louie, arXiv:1705.04245.
[52] A. Marini and R. Del Sole, Phys. Rev. Lett. **91**, 176402 (2003).
[53] C. Blomberg and B. Bergersen, Can. J. Phys. **50**, 2286 (1972).
[54] F. Aryasetiawan and O. Gunnarsson, Rep. Prog. Phys. **61**, 237 (1998).
[55] M. Vos, A. S. Kheifets, E. Weigold, S. A. Canney, B. Holm, F. Aryasetiawan, and K. Karlsson, J. Phys.: Condens. Matter **11**, 3645 (1999).
[56] A. S. Kheifets, V. A. Sashin, M. Vos, E. Weigold, and F. Aryasetiawan, Phys. Rev. B **68**, 233205 (2003).
[57] M. Guzzo, G. Lani, F. Sottile, P. Romaniello, M. Gatti, J. J. Kas, J. J. Rehr, M. G. Silly, F. Sirotti, and L. Reining, Phys. Rev. Lett. **107**, 166401 (2011).
[58] F. Bechstedt, M. Fiedler, C. Kress, and R. Del Sole, Phys. Rev. B **49**, 7357 (1994).

[59] S. Baroni, S. de Gironcoli, A. Dal Corso, and P. Giannozzi, Rev. Mod. Phys. **73**, 515 (2001).
[60] M. Lazzeri, C. Attaccalite, L. Wirtz, and F. Mauri, Phys. Rev. B **78**, 081406(R) (2008).
[61] C. Faber, J. L. Janssen, M. Côté, E. Runge, and X. Blase, Phys. Rev. B **84**, 155104 (2011).
[62] B. Monserrat, Phys. Rev. B **93**, 100301(R) (2016).
[63] Z. Li, G. Antonius, M. Wu, F. H. da Jornada, and S. G. Louie, Phys. Rev. Lett. **122**, 186402 (2019).
[64] F. Karsai, M. Engel, E. Flage-Larsen, and G. Kresse, New J. Phys. **20**, 123008 (2018).
[65] J. Sak, Phys. Rev. Lett. **25**, 1654 (1970).
[66] M. Matsuura and H. Büttner, Solid State Commun. **33**, 221 (1980).
[67] A. S. Davydov, Phys. Status Solidi **20**, 143 (1967).
[68] T. Takagahara, Phys. Rev. B **31**, 6552 (1985).
[69] J. Singh, *Excitation Energy Transfer Processes in Condensed Matter Theory and Applications* (Plenum, New York, 1994).